Designing an irreversible metabolic switch for scalable induction of microbial chemical production

Ahmad A. Mannan[1] **and Declan G. Bates** [1,†]

December 18, 2020

[1] Warwick Integrative Synthetic Biology Centre, School of Engineering, University of Warwick, Coventry, CV4 7AL, UK.

[†] Correspondence to D.Bates@warwick.ac.uk

Abstract

Bacteria can be harnessed for the synthesis of high-value chemicals. A promising strategy for increasing productivity uses inducible control systems to switch metabolism from growth to chemical synthesis once a large population of cell factories are generated. However, chemical induction via IPTG and other gratuitous inducers is extremely expensive, limiting the scaleability of this approach for biotechnological applications. Switching to production using cheap nutrients is an appealing alternative strategy, but their uptake is tightly regulated, and since they are metabolised, sustaining induction requires their constant addition, again limiting scalability. Here we develop a mathematical model of fatty acid uptake in *E. coli* as an exemplary case study, and use it to study how the cell's native regulation and program of induction can be engineered to minimise inducer usage. We show that augmenting the native control circuitry with positive feedback loops creates an irreversible metabolic switch, which requires only temporary induction, drastically reducing total inducer usage. Our proposed switch should be widely applicable, irrespective of the specific product of interest, bringing closer the realisation of scalable and sustainable production of high-value chemicals from microbes.

1 Introduction

Bacteria use highly complex control systems to orchestrate their metabolism in response to changing environmental stimuli or to take advantage of nutrients when they become available. Recent advances in synthetic biology are enabling the re-design of native bacterial control systems, and there is strong interest in applying this approach to modify metabolism and create *microbial cell factories* with improved production of high-value chemicals [1, 2]. The seminal theoretical work of [3, 4] demonstrated that a two-stage strategy can decouple metabolic objectives and overcome the inherent trade-off between cell growth and chemical synthesis. Cells first express a *growth phenotype* so a large population of factories are generated, then they are induced to switch to a *production phenotype* for chemical synthesis. Applications of this strategy, known as dynamic control, have harnessed chemically-responsive transcription factors to induce the switch, and reported improved titres and volumetric productivity [5, 6]. This strategy promises to be especially advantageous in situations where growth has to be severely sacrificed for product synthesis [7].

Recent studies have successfully engineered dynamic control using IPTG-inducible LacI [8, 9]. However, the use of IPTG and other gratuitous inducers is extremely expensive (e.g. £1055 for 25g IPTG, $\geq$99% purity, SigmaAldrich), and quickly becomes economically infeasible when scaled-up for industrial applications. Moreover, these inducers exhibit toxicity at high concentrations [10], which can negate production capacity. Alternatives include the use of physical stimuli such as glucose-starvation [11] and temperature change [12], and the use of quorum-sensing systems for autonomous induction at a pre-set threshold population density [13, 5, 6]. However, physical stimuli could cause unintended global metabolic changes that impair production capacity, and quorum-sensing requires constant inducer presence to retain the induced state. After shifting to production, autoinducer synthesis may cease, and its decay means an eventual loss of induction and a shorter production phase.

Hence, the simplicity of manual induction remains attractive, particularly for implementation in industry, where existing processes can easily be adapted to this regime. Achieving optimal productivity does require careful timing of induction [3, 13], but this is easily done by tracking culture density. A more fundamental problem is the high cost of chemical induction, which severely limits the scalability of this approach to large-scale biotechnological applications - how to reduce the total amount and cost of inducer used over the whole production process remains the key challenge.

To address the costs of using expensive gratuitous inducers, we instead look at exploiting cheap, natural

nutrients such as fatty oleic acid to induce the switch from growth to production. Bacteria can take advantage of oleic acid when it becomes available, but its uptake and use is tightly regulated. Transcription factor FadR represses the expression of enzymes that catalyse its uptake (FadD) and degradation (FadE), as well as itself (autoregulation) (Fig.1(a), endogenous system). When oleic acid becomes available, a small amount is internalised (acyl-CoA) and sequesters FadR, relieving its repression and allowing further uptake. This control system is a recurrent strategy, with a number of other nutrients able to induce their own uptake and control gene expression in the same way in *E. coli* (Table S1). By extending their control on the expression of enzymes driving growth and production (Fig.1(a), control application), we can implement dynamic control. However, nutrients are metabolised, so sustaining induction requires their constant addition. This is not scalable, even if a cheap inducer is used.

To address this problem, we hypothesised that re-engineering this control system to behave as a bistable switch will reduce the amount of inducer needed. Bistable switches endow a *memory* of the induced phenotype [14], enabling cells to retain the production phenotype even after reducing the amount of inducer. A fundamental design principle for bistability is positive feedback [15, 16], and this is an integral feature of nutrient uptake regulation circuitry (Fig.1(a), dashed arrow). Furthermore, if the bistable-switch can be made irreversible, only temporary induction will be needed to switch to and remain at the production phenotype. This means we can prolong production without further induction and skip costly batch culture restarts to further lower total amount and costs of induction. However, it is not currently known how to engineer a nutrient uptake system to behave irreversibly.

Here, we look at the oleic acid-inducible fatty acid uptake system from *E. coli* DH1Δ*fadE* strain used in [17] (Fig.1(a), cross), as an exemplary case study of a nutrient uptake system. This strain has recently been shown to have a slower reversion back to the uninduced state vs its parent DH1 strain [17], and this desirable property for our application makes it a good starting point in our engineering effort. We developed a mathematical model of this system and used it to study how to design a bistable controller that switches irreversibly from the growth phenotype with high growth rate, to the production phenotype with low growth rate. We exhibit control designs and optimal induction regimes that minimise both total inducer used and the time to switch to the production phenotype, in the face of a reduced growth rate during induction. We find that modifying the native circuit topology so that FadR activates its own expression produces a more robust bistable switch, that requires less inducer to achieve the production phenotype and even less to sustain it. However, by augmenting the circuitry with another positive feedback loop we show that the bistable switch can behave irreversibly and drastically lower induction costs. Simulations of the induction dynamics

during feed-batch culture reveal an inherent trade-off between the total inducer used over the process and time to achieve the production phenotype, but we found simple principles to improve the induction process performance: reducing inducer feed-in rate to an optimal level reduces total inducer usage, and increasing availability of uptake enzyme FadD prior to induction shows an earlier switch to the production phenotype.

2 Results

2.1 Designing a robust bistable-switch

We first study how to re-engineer the fatty acid uptake system and its control on growth and production (Fig.1(a)) to make it behave as a bistable switch. For this, we developed a mathematical model of the system, the equations of which are given in Methods and the details of its formulation and parameterisation given in S2. We used our model to study how modifying the autoregulation of sensor-regulator FadR, that is how it regulates its own expression, and how tuning circuit parameters affects the switch behaviour, which we characterise with the system dose-response. As defined in Methods, this shows the state of the system, which we define as the concentration of FadR, achieved at different doses of the inducer oleic acid (OA) (Fig.1(b)). However, we focus the switch characterisation on three key features of the dose-response curve: the induction threshold, reversion threshold, and bistable range (Fig.1(b), see Methods).

In our engineering effort, we consider two forms of the FadR autoregulation: its native negative autoregulation (NAR), and its positive autoregulation (PAR) (Fig.1(a), right). It has recently been reported that modifying FadR with PAR slows the time it takes for the fatty acid uptake system to revert back to its uninduced state [17]. This is a desirable property for our application and so an important circuit topology to consider. For the system parameters, we focus on exploring only those parameters that are easily modified in the lab. It is well established that by altering the location, number and DNA sequence of an operator site for TF binding, or modifying the sequence of the RNAP binding sites, one can modify the level of leaky expression of a repressed gene, its promoter strength, and affinity the TF binds its operator upstream of the gene [18, 19]. We therefore limit our engineering effort to focus on modifying the expression leakiness (b_R, b_D) and promoter strengths of TF FadR and uptake enzyme FadD (a_R, a_D), and the affinity FadR binds its operator on its own promoter and that of *fadD* (K_R, K_D).

To achieved a bistable switch our global sensitivity analysis (see Methods) revealed that we did not need to explore all six parameters, but could focus on two key *tuning dials*. Specifically, the induction threshold

and bistable range are most sensitive to changes to the FadD expression leakiness (b_D), and the reversion threshold is most sensitive to changes to the FadD promoter strength (a_D) (Fig.S2(a)). By varying a_D and b_D between 10–1000% of their nominal value, we discovered the circuit with PAR has a larger range of parameters where the switch is bistable, with a lower induction threshold and even lower reversion threshold, vs the native circuit with NAR (Fig.1(c), dose-responses in Fig.S2(c)). In other words, we can engineer a robust bistable switch that needs less nutrient to induce the production phenotype, and even less to maintain it.

In our circuits, the cell's growth rate is also controlled. Based on the data from Usui *et al.* [20] (see S2), we used a linear equation (Eq.8) to model growth rate dependence on a growth-associated enzyme E_g, which for example could be glucose-6-phosphate isomerase from upper glycolysis [20], whose expression is in turn activated when FadR is available. During induction, FadR is sequestered and growth is subsequently attenuated, but since this affects the dilution of all other species in the system we wanted to understand how this feed back affects the switch behaviour. Interestingly, we found that for a greater proportional drop in growth after induction (higher s_T values), the lower the induction and reversion thresholds, irrespective of the circuit topology (Fig.1(d), dose-responses in Fig.S2(b)). Though both are affected, our global sensitivity analysis indicates that reversion threshold is decreased most (Fig.S2(a)). This helps to reinforce the bistable nature of the switch, and makes it well suited to enact the dynamic control strategy, which is particularly advantageous when growth needs to be severely sacrificed for production [7].

2.2 Tuning induction regime to sustain induced state

We now apply our two circuits to switch from the growth to production phenotype during the feed-batch production phase, once enough cell factories have been generated and we start to introduce OA to induce the switch. We extended our model to simulate the dynamic availability of OA (Eqs.9) and define the induction program in Eq.10 (see Methods), and used it to elucidate how to tune the induction program and engineer the switches parameters to address our induction performance objectives: to minimise (i) total OA used over a 100 hours of the process, and (ii) the time the system first reaches the production phenotype, i.e. the switch time.

First keeping fixed the control system parameters to their nominal values, we studied how our induction performance is affected by varying the key induction tuning dial, the feed-in flux f (Eq.10), from 0.25–

5μM/h. That is, we solved the multi-objective optimisation problem:

$$\begin{aligned} &\min_f (J_1, J_2)\,, \\ &\quad J_1 = \int_{t=0}^{100} f_{\text{in}}(t)\,\text{dt}; \quad J_2 = \min\left(t \mid R(t) \leq R_{pp}\right); \\ &\quad \text{subject to } 0.25\mu\text{M/h} \leq f \leq 5\mu\text{M/h}, \end{aligned} \tag{1}$$

where R_{pp} is the highest concentration of FadR for which the system is defined to be at the production phenotype (see Methods). This gave us a set of Pareto solutions that revealed an inherent trade-off between the two objectives: slower feed-in results in less total OA used, but at the cost of longer times to switch to the production phenotype (Fig.2(a)). An optimal feed-in flux can be selected to balance the objectives and give a performance closest to the utopia (0,0), but interestingly the control with PAR showed a larger range of feed-in flux values where less OA is used or the switch time is less, vs circuit with NAR (Fig.2(a)).

To unravel what is behind this superior performance, we selected feed-in flux f=1.3μM/h (Fig.2(b), top plots) and simulated the induction dynamics for both circuits. Simulations revealed three fundamental differences in the dynamic response by the system with PAR vs NAR: (i) it reaches the induced state earlier (Fig.2(b), τ), (ii) retains that state for longer (Fig.2(b),$*$), and (iii) the length of subsequent inductions needed to sustain that state are shorter (Fig.2(b),$\dagger$). The key factor driving these behaviours is the lower concentration of total FadR ($R + C$) in the system after it is induced (Fig.2(b), bottom plots). During induction, almost all free FadR (R) are stored into an inert sequestered complex (C) (Fig.2(b), second and fourth bottom plots), and once induction ceases sequestration is reversed and FadR is quickly freed to again repress expression of the unneeded FadD. However, in the system with PAR, FadR's sequestration during induction impairs its self-activation, as opposed to the enhanced expression seen in the circuit with NAR (Fig.2(b), fourth vs second bottom plot). This means there is far less FadR to sequester in the system with PAR, and so consequently reaches the production phenotype earlier. Furthermore, since continued growth progressively dilutes away the pool of total FadR stored as sequestered complex, less and less FadR is freed every time induction is ceased. Less FadR does mean shorter subsequent induction periods are needed to sustain the production phenotype, but also the resulting weaker self-activation causes the observed slower reversion ((Fig.2(b), bottom far right plot)).

The slower reversion is in fact an emergent property of the circuit with PAR, not simply caused by a choice of parameters. We define the reversion rate mathematically as the least negative eigenvalue of the system dynamics close to the uninduced steady state (growth phenotype), and from the eigenvalues we derived in

terms of the system parameters (see S4), we find that the reversion rate of the circuit with PAR is always slower than that of the circuit with NAR, irrespective of the parameters (as long as they are positive valued).

To elucidate the principles of how to engineer our two switches to further reduce total OA used over the induction process, we then varied each experimentally accessible parameter at a time ($b_R, a_R, K_R, b_D, a_D, K_D$), from 100% to 1% of their respective nominal value in Table S2, and recalculated the performance objectives of the Pareto solutions. We found the Pareto was almost unaffected by our variations in the expression and regulation of FadD (b_D, a_D, K_D) (Fig.S3), but was sensitive to changes in the expression and regulation of FadR, particularly in the circuit with FadR PAR. Specifically, a further reduction in total OA used can be achieved by an effective lowering of the amount of FadR, by reducing FadR promoter strength (a_R), or by decreasing affinity to self-activate (K_R), but an inherent limit was observed (Fig.2(a), inset plots). Intuitively, if we reduce these parameters there will be very little FadR, which will effectively break our control system.

2.3 Additional positive feedback loop enables irreversibility

We next investigated whether the bistable-switch could be engineered to behave irreversibly, that is to retain the induced state even after inducer is completely removed. That way, no further inductions will be required beyond an initial period, and will drastically reduce total induction costs over a long production process.

Mathematically, a bistable switch can behave irreversibly if it can achieve more than one stable steady states when there is no inducer. Our mathematical analysis in Supplementary S6 proves that in fact this is not possible for either the system with NAR or PAR. A change in circuit topology is required.

For irreversibility, we need FadR to remain inactive after induction ceases. This requires a combination of two steps: (i) depleting the total pool of FadR (free FadR R and complex C) during induction, and (ii) repressing further expression of FadR after induction ceases. We have shown that the circuit with PAR can achieve step (i), but to fulfil step (ii) we raise the hypothesis that addition of the mutual inhibition of FadR and another TF, such as TetR (Fig.3(a)), can achieve this. Our intuition is that during induction FadR's sequestration will allow TetR expression, which in turn will suppress further FadR expression and cause its depletion. Once induction ceases, there wont be enough FadR to repress its repressor TetR again, allowing us to retain suppression of FadR expression and so prevent reversion. However, enough of an induction period has to have been allowed to sufficiently deplete the pool of FadR.

To test our hypothesis, we developed a model of our proposed switch circuit topology illustrated in Fig.3(a).

It is the same as Eqs.(5), (7) and (8), except we now model expressions of FadR (R) and TetR (T) with:

$$\begin{aligned} \frac{dR}{dt} &= b_R + P(R,T) - k_f A^2 R + k_r C - \lambda R \\ \frac{dT}{dt} &= b_T + \frac{a_T}{1+(K_{Ri}R)^2} - \lambda T. \end{aligned} \tag{2}$$

Here, $P(R,T)$ models the expression of FadR, which can be a function of only TetR (NoPAR, Fig.3(a), right) or both FadR and TetR. When dependent on both transcription factors, their operator sites can be arranged so their binding is competitive (Comp) or non-competitive (NonComp) (Fig.3(a), right). This gives us three possible circuit topologies to explore, and for each we derived the corresponding formula to model the FadR and TetR dependent expression of FadR as:

$$\begin{aligned} \text{NoPAR:} \quad P(T) &= \frac{a_R}{1+(K_T T)^2}, \\ \text{Comp:} \quad P(R,T) &= \frac{a_R K_R R}{1+K_R R+(K_T T)^2}, \\ \text{NonComp:} \quad P(R,T) &= \frac{a_R K_R R}{(1+K_R R)(1+(K_T T)^2)}, \end{aligned} \tag{3}$$

(see S7 for derivations and parameterisation), the parameters of which are based on characterised parts in the literature (Table S4).

To understand whether the proposed circuit topologies could behave irreversibly, we attempted to solve our systems analytically for the steady states in terms of the parameters at OA = 0μM. Though the equations derived (Eq.S23) cannot be solved analytically, we note that its solution would give us steady states of FadR in terms of primarily those parameters of the expression and regulation of FadR and TetR (see S7.5): $b_R, a_R, K_R, b_T, a_T, K_{Ri}, K_T$. Interestingly, irreversibility does not depend on FadD expression (b_D, a_D, K_D), or the reaction kinetics of FadD ($k_{\text{cat,D}}, K_{\text{m,D}}$), PlsB ($k_{\text{cat,D}}, K_{\text{m,D}}$) or sequestration ($k_f, k_r$).

To uncover the parameter regimes that achieve irreversibility, we explored a four-dimensional design space of experimentally-accessible parameters a_R, a_T, K_T, K_{Ri}, varying all parameters simultaneously between 10^{-3}–10^3 times their respective nominal values from Table S4. We found all three proposed circuits can be engineered to behave irreversibly, with the Comp circuit showing the largest parameter space in which we can design this behaviour (Fig.3(b) vs Fig.S6), i.e. the most robust design. Nevertheless, the design principles are similar between the three circuits. In particular, based on parameter values of characterised parts from the literature, we see that engineering stronger promoter strengths of both FadR and TetR (a_R, a_T) are needed. Also, we need to weaken the affinities of each transcription factor to inhibit the others expression, though a stronger transcriptional inhibition of TetR expression by FadR (K_{Ri}) is needed vs that on FadR expression

by TetR (K_T) (Fig.3(b)). There is however a sweet-spot. If K_T is weakened too far we lose the irreversibility (Fig.3(b), $a_T - K_T$-plane) because this effectively breaks the positive feedback in the mutual FadR-TetR inhibition and leaves us with the circuit with FadR PAR, which we know is not irreversible (Fig.4(c), grey curve).

We highlight an example parameter regime that enables all three circuits to behave as irreversible switches (Fig.4(b) and (c), green dot and curve), and detail in Table S4 a proposal for how to engineer an irreversible switch with the Comp circuit (most robust design) in the lab. We will hereafter refer to this engineered system as *our irreversible switch.*

2.4 Tuning induction and switch to minimise inducer use

We now apply our engineered control system to irreversibly switch from growth to production during a feed-batch induction process, and revisit our question of how tuning the induction regime and parameters of our irreversible switch affect the induction performance.

We model dynamic availability of OA again by Eq.9, but the irreversible switch behaviour now requires a different OA feed-in program f_{in}. Instead of an intermittent addition based on sensing of FadR concentration, we only induce once, but now have two tuning dials: (i) the OA feed-in flux f, and (ii) the time length it is added for, i.e. exposure time t_{exp} (Fig.4(a)). We define this induction program in Eq.11 (see Methods). Focusing first on exploring f and t_{exp} for fixed control parameters, we evaluated the following multi-objective optimisation problem to find optimal induction programs that minimise our induction performance objectives: OA used (J_1) and switch time (J_2):

$$\begin{aligned} &\min_{\underline{c},f} \left(J_1, J_2\right), \\ &\quad J_1 = \int_{t=0}^{100} f_{\text{in}}(t)\,\text{dt}; \quad J_2 = \min\left(t \mid R(t) \leq 0.05\mu M\right), \\ &\quad \text{subject to} \quad 1\mu M \leq f \leq 50\mu M; \quad 0.1\text{h} \leq t_{\text{exp}} \leq 5\text{h}. \end{aligned} \tag{4}$$

For our switch with given parameters, we define the production phenotype when FadR $\leq 0.05\mu$M , which can be seen on the dose-response curve in Fig.4(c) (green curve).

Solving Eq.4, we again find a Pareto front of solutions that reveal a trade-off between our two performance objectives, though interestingly, we find designs that drastically lower OA usage but make little difference to switch times (Fig.4(b)). Here, reducing total OA used is achieved primarily by reducing exposure time, without needing to alter feed-in flux (Fig.4(b), right plots), though a minimum exposure time is required. These key principles enable us to set an induction program with far superior performance, i.e. lower inducer

use and switch times, than those possible with the reversible bistable-switch seen in Fig.2(a).

To elucidate how the induced state is retained after the induction period, we simulated the induction response dynamics for an example optimal induction program, where f=45.6μM/h and t_{exp}=0.31h, (black dot in right plots of Fig.4(b)). We found that during induction a high level of OA is rapidly accumulated thanks to high feed-in flux (Fig.4(a)). This allows for the continuation of FadR sequestration into complex form, long after the induction period has ended. This in turn grants enough time for free FadR levels to fall and allow expression of TetR. When there is no more OA, some FadR is freed from the complex, and though it does repress TetR expression temporarily causing a dip in available TetR, it is insufficient to activate further expression of FadR and lockdown TetR expression. This results in FadR diluting away, allowing further TetR to be expressed and resulting in an effective lockdown of FadR expression.

We then looked at how tuning parameters of the irreversible switch affect performance of the induction process. We varied each of the experimentally-accessible parameters in turn by $\pm 25\%$ of their engineered values (Table S4), and recalculated the total OA used and switch time, for each of the optimal induction programs of the Pareto front in Fig.4(b). We find that it is primarily the switch time that can be tuned by tuning the parameters, with little effect on total OA used (Fig.S7). Interestingly, the switch time is most sensitive to changes in the amount of FadR and leakiness of FadD expression. In particular, tuning down FadR promoter strength (a_R), strength of PAR (K_R), or increasing FadR repression by TetR (K_T) is most effective at reducing switch times (Fig.S7). Similarly, increasing the leaky expression of uptake enzyme FadD enables a large drop in switch time too (Fig.4(b), inset). Since reducing FadR by weakening a_R or K_R goes against the principles we deduced for tuning the system to achieve an irreversible switch, and tuning FadD expression does not affect that ability, we infer the key handle on switch time is therefore FadD leakiness (b_D). We infer that the key principle to reducing switch time is thus speeding the uptake of more acyl-CoA, to sequester away more FadR earlier.

There is a key design constraint though. For designs with lowest total OA used, parameter tuning can cause the optimal induction regime to no longer be sufficient to keep the system at the induced state (lines that shoot up on left side of plots in Fig.S7). Since this problem was not as apparent for those induction programs with slightly higher total OA used, we suggest a pragmatic approach to overcoming this problem: select a slightly suboptimal induction program. As elucidated in the previous section, one must also beware that tuning parameters too far may make the switch behave reversibly again.

3 Discussion

In this work, we have elucidated how to redesign the native regulation of fatty acid uptake in *E. coli*, and create a dynamic control mechanism that takes advantage of nutrient oleic acid to irreversibly switch cell metabolism from growth to production. Most importantly, since this means the induced state is retained after a single, short induction with a cheap nutrient, our proposed control design drastically cuts induction costs. This allows for an economically-viable scaling of induction, addressing the fundamental impediment to implementing dynamic control for industrial-scale production.

Dynamic control is a recently proposed strategy that enhances productivity (titres per unit time) from cell factories where growth has to be severely sacrificed for chemical synthesis [4, 7]. Recent advances in synthetic biology have enabled inducible control systems from bacteria to be repurposed for implementing dynamic control [2, 17]. However, they do require a constant inducer presence to retain the induced state, and this is not scalable even with the use of cheap inducers. Given the ultimate purpose of developing cell factories is for industrial production, in this study we asked how to design a dynamic control switch that can minimize inducer usage. Moreover, since design of the switch will affect and be affected by how we implement the induction process [17], we studied both the switch design and a feed-batch induction program using a mathematical model of fatty acid uptake and it's control on growth, as our model system.

We showed that the endogenous system can be tuned to behave as a bistable switch, but found that altering the native circuit topology so FadR expression is positively autoregulated (PAR) rather than negatively autoregulated (NAR), grants a more robust and superior switch. That is, there is a larger design space where it is bistable and requires less oleic acid to achieve the induced state. Moreover, simulations of the feed-batch induction dynamics discovered that the control with PAR needed shorter intermittent exposures of inducer and retained the induced state for longer, irrespective of the control parameter values, resulting in a lower total OA usage during the process, and reinforcing the superiority of the switch with PAR above the native design. Our analysis unveiled that the fundamental reason why we needed less inducer was because of the eventual dilution of FadR via cell growth and division. During induction sequestered FadR cannot activate its own expression, causing pools of FadR, whether sequestered or free, to dilute away. Once induction is ceased, there is insufficient FadR to quickly revert the system, which is diametrically opposite to the very behaviour nature had optimised the native fatty acid uptake system for [17].

As desirable as the switch with PAR is, we proved that it cannot behave irreversibly and so always needs to

be intermittently induced. We did discover that addition of another positive feedback loop, through mutual inhibition between FadR and another TF TetR, enables us to engineer an irreversible switch. The key design principles for irreversibility are stronger promoter strengths of FadR and TetR, but weakened affinities of each to bind and inhibit the others expression. However, there is a sweet-spot - if TetR inhibition of FadR expression is too weak the feedback breaks and so to does irreversibility. Interestingly, by arranging the FadR and TetR operator sites regulating the expression of FadR so that FadR and TetR bind competitively (only one at a time) we found a larger design space in which to engineer for irreversibility.

Application of the irreversible switch for dynamic control was far easier to implement than for the reversible switch. Since only a predetermined short initial induction period is needed there is no requirement to sense the state of the system to decide when to add or cease induction - greatly simplifying implementation of the induction process. However, this did mean we had two dials for its implementation, inducer feed-in flux and time length of induction. Interestingly, we found that it is by tuning down primarily the exposure time that we could minimise the total OA used. Moreover, since this did not affect the switch time much, we discovered that the main handle on that objective lies in tuning the parameters of the irreversible switch. In particular, we found that increasing FadD expression leakiness to allow a greater uptake flux of OA and earlier sequestration of FadR could drastically reduce the switch time. The cost of this modification is that we may need to select a slightly longer exposure time to ensure that FadR is sufficiently depleted and enough TetR is expression to keeps FadR expression locked-down.

In our elucidation of the design principles for constructing an irreversible switch in the lab, we did focus on those parameters that are easily modified in the lab. Nevertheless, our mathematical analysis did reveal that in fact achieving irreversibility is not dependent on the parameters associated with the expression and regulation of uptake enzyme FadD, nor on the reaction kinetics of inducer uptake, consumption or sequestration. It is with this powerful insight we speculate that many other nutrient uptake system native to *E. coli*, that share the same control circuit topology as our fatty acid system (listed in Table S1), may also be engineered as irreversible switches by the same design principles. However, when constructing the proposed switch in the lab two important interventions also need to be implemented: (i) knocking-out degradation enzyme like FadE (hence our focus on *E. coli* DH1Δ*fadE* strain (Fig.1a)), to reduce consumption of inducer and allow shorter induction exposure periods; and (ii) engineer the promoter of uptake enzymes like FadD to allow expression without the need for activation by CRP-cAMP, to make the switch independent of growth media. Coregulation by carbon catabolite repression is a common feature of a number of the nutrient uptake enzymes in *E. coli*. In the case of fatty acid uptake, if *E. coli* is cultured on glucose, expression of FadD is

inactive, and little oleic acid will be taken up when available, impairing the switch function. We suggest to replace FadD promoter with a synthetic promoter with only an operator for inhibition by FadR.

There are a few caveats to bear in mind when constructing our circuit in the lab. Though we discovered a more robust design for the irreversible switch with the addition of FadR PAR, protecting its function against the deleterious effects of genetic drift poses a challenge in the long run. Harnessing the principle of growth-coupling may help. FadR's activation of E_g in our circuit creates growth-coupling, and we speculate this at least creates selection pressure to preserve our circuit's control on growth. Furthermore, if our circuit control's expression of the right host-native enzymes during induction to create growth-coupled production [21], this may also confer selection pressure to preserve the circuit function. Another important point of consideration is the burden of expressing the heterologous product synthesis pathway enzymes. Their expression may compete for endogenous ribosomes and RNAP [22] and in turn affect our circuit's function [23, 24, 25]. However, since reducing cell growth rate increases the proportion of ribosome content [26], we speculate that the sacrifice of growth for production enacted by our control switch may be helping relieve competition for ribosomes. Alternatively, applying an orthogonal ribosome system to control expression of the heterologous enzymes has recently been shown to help relieve such competition [27]. It is also important to consider how sequestering a TF such as FadR can affect other parts of metabolism. In our case, sequestering FadR may affect its activation of the fatty acid biosynthesis regulon [28], an essential pathway, and repression of the glyoxylate shunt [29] in *E. coli*. However, in the study of Hartline et al [17] there was no evidence the rate of growth on a glycerol media was affected when FadR was sequestered with OA. Moreover, since our switch will decrease growth, the demand for these pathways will decrease anyway, and so we speculate that the switch function will not affect those pathways much.

Our study has important implications for synthetic biology, this being the first time design of an inducible and irreversible metabolic switch has been proposed. This study also directly contributes to metabolic engineering efforts. Our proposed control switch serves as a mechanism to implement the dynamic control strategy for microbial production, irrespective of the specific chemical product of interest, and in a scalable and economically viable way. This is especially important for application to industrial biotechnology, bringing closer the realisation of scalable and sustainable production of high-value chemicals from microbes.

4 Methods

4.1 Model of fatty acid-induced switch from growth to production

We developed a model of the dynamics of our oleic acid-inducible control system as a system of ODEs. Full details of its formulation and parameterisation can be found in S2, but we outline the model equations here. The model is of two parts: (i) the native fatty acid uptake system, from *E. coli* DH1Δ*fadE* strain (Fig.1(a), endogenous system), and (ii) the control of oleic acid-responsive transcription factor (TF) FadR on the expression of enzymes directly affecting growth and production (Fig.1(a), green arrows).

The first part of our model is adopted from Hartline and Mannan *et al.* [17], and models the expression of TF FadR (R) and uptake enzyme FadD (D), and their control as a function of FadR, and the dynamic availability of fatty acyl-CoA (A) and acyl-CoA-sequestered FadR complex (C) as follows:

$$\begin{aligned}
\frac{dR}{dt} &= b_R + P_R(R) - k_f A^2 R + k_r C - \lambda R, \\
\frac{dD}{dt} &= b_D + \frac{a_D}{1 + (K_D R)^2} - \lambda D, \\
\frac{dA}{dt} &= \frac{k_{cat,D} \cdot \mathrm{OA}}{K_{m,D} + \mathrm{OA}} \cdot D - \frac{k_{cat,B} \cdot A}{K_{m,B} + A} \cdot B - 2 \cdot \left(k_f A^2 R - k_r C\right) - \lambda A, \\
\frac{dC}{dt} &= k_f A^2 R - k_r C - \lambda C,
\end{aligned} \tag{5}$$

where $P_R(R)$ models the autoregulation of FadR. In our study we consider two configurations of FadR autoregulation: (i) its negative autoregulation (NAR), as is in the native circuitry, and (ii) its positive autoregulation (PAR), as engineered in [17] (Fig.1(a), right), and model them as:

$$\begin{aligned}
\mathrm{NAR}: \ P_R(R) &= \frac{a_R}{1 + K_R R}, \\
\mathrm{PAR}: \ P_R(R) &= \frac{a_R K_R R}{1 + K_R R}.
\end{aligned} \tag{6}$$

The second part of our model captures the control of FadR on growth. We first model the FadR-activated expression of a growth-associated enzyme E_g as:

$$\frac{dE_g}{dt} = \frac{a_g K_g R}{1 + K_g R} - \lambda(E_g) \cdot E_g, \tag{7}$$

and then used a linear equation to phenomenologically model growth rate as a function of E_g:

$$\lambda = \lambda_{\max} \cdot \left(1 - s_T \cdot (1 - E_g)\right), \tag{8}$$

where $s_T = 1 - \frac{\lambda_{\min}}{\lambda_{\max}}$ represents the *severity* of growth attenuation or the proportional drop in growth rate when E_g is no longer expressed, and $\lambda_{\min}$, $\lambda_{\max}$ represent growth rates at zero and max expression of E_g.

This phenomenological model of growth was derived using data from the experiments of Usui, *et al.* [20], who showed that for successive decreases in the expression of upper glycolysis enzyme glucose-6-phosphate isomerase (Pgi) growth rate decreased linearly (see S2).

To keep our model independent of the specific product of interest, and a minimal description of our system, we did not model the expression and control of a product synthesis enzyme E_p. Its expression is exclusively dependent on FadR and does not feedback onto the system. We instead define the production phenotype by a low concentration of FadR, $R = 0.0033\mu$M. This assumes the FadR operator upstream of gene encoding E_p is engineered to be that upstream of *fadD*, and represents the FadR concentration threshold that achieves the concentration of the respective gene product that is halfway between its min and max.

4.2 The dose-response to characterise switch behaviour

We characterise the switch behaviour from a plot of the dose-response curve (Fig.1(b)), generated by solving for the steady states of FadR at logarithmically spaced set values of inducer OA. We determined them numerically, first deriving a nullcline in terms of FadR and model parameters for each of our models system (see S2.4 for the reversible switch model and S7.4) for the irreversible switch model), then using bisection as a method to determine the steady states at its roots. To determine their stability nature, we substituted the steady state values into the analytically derived Jacobian matrix, and solved for its eigenvalues. If all eigenvalues have a negative real part, with at least one eigenvalue with a non-zero real part, then we defined that steady state stable (solid part of dose-response curve), else if at least one eigenvalue had a positive non-zero real part then we defined that steady state unstable (dashed part of dose-response curve).

We used the dose-response to distinguish between switch designs, and measured three key features of the curves: (i) the induction threshold, the concentration of OA needed to switch the system to the production phenotype; (ii) the reversion threshold, the highest concentration of OA needed to revert back to the growth phenotype; and (iii) the bistable range, the range of OA concentration where the system can be in one of two possible phenotypic state (Fig.1(b)).

4.3 Global sensitivity analysis

In our study of how the system parameters of the endogenous system in Fig.1(a) affect the dose-response curve, we looked to first determine those parameters for which the induction threshold, reversion threshold and bistable region are most sensitive. To determine those parameters we applied the method of the extended

Fourier Amplitude Sensitivity Test, or eFAST, using the MATLAB toolbox published in [30]. The method generated 100 random sets of the experimentally accessible parameters b_R, a_R, K_R, b_D, a_D and K_D between 10% to 500% of their respective nominal values in Table S2, and the proportional drop in growth rate parameter s_T between 0.1 and 0.9, and calculated the first-order sensitivity indices. Due to the random nature of the sampling, we repeated this three times and calculated the average and standard deviation of the sensitivity indices for each parameter (Fig.S2).

4.4 Simulating induction dynamics during production phase

To simulate induction dynamics, we extend our models to incorporate dynamic availability of OA with ODE:

$$\frac{d\mathrm{OA}}{dt} = f_{\mathrm{in}} - \frac{k_{cat,D} \cdot \mathrm{OA}}{K_{m,D} + \mathrm{OA}} \cdot D. \tag{9}$$

The second term refers to the specific consumption rate of inducer, and f_{in} states OA feed in regime, which we now define. For the reversible switch, our induction process involves a FadR-dependent intermittent feed of OA to retain the production phenotype. We feed in OA at a fixed flux of $f\mu$M/h and cease it once enough FadR is sequestered that its concentration falls well below the concentration that qualifies the cell being in the production phenotype, which we define as FadR $\leq 0.3 \times 0.0033\mu$M. It is important to note that the precise scaling factor of 0.3 does not change our results, as long as it is < 1. When induction is ceased, the reversible nature of the switch means the system starts to revert back to the growth phenotype. To sustain the production phenotype, further OA is intermittently added at $f\mu$M/h, and we define this induction program:

$$f_{\mathrm{in}}(R) = \begin{cases} f \in \mathbb{R}^+, & \text{for } R > 0.0033\mu\mathrm{M/h}, \\ 0, & \text{for } R \leq 0.3 \times 0.0033\mu\mathrm{M/h}. \end{cases} \tag{10}$$

In the case of the irreversible switch, only a single initial period of OA feed-in is required at flux $f\mu$M/h, and for time length, or exposure time period t_{exp}. We define this induction regime as:

$$f_{\mathrm{in}}(t_{\mathrm{exp}}) = \begin{cases} f \in \mathbb{R}^+, & \text{for } t \leq t_{\mathrm{exp}}, \\ 0, & \text{for } t > t_{\mathrm{exp}}. \end{cases} \tag{11}$$

4.5 Multi-objective optimisation

In implementing the induction process, we explored how to tune induction and the control circuit parameters, within bounded intervals of each of their values, with the aim of minimising two key induction process performance objectives: (i) total OA used over a 100 hours of the induction process (Eq.10), and (ii) first time the system reaches the production phenotype, or switch time. We posed this as a multi-objective

optimisation problem, formally stated in Eq.1 for the reversible switch, and Eq.4 for the irreversible switch, and used the `gamultiobj` function from the Global Optimization Toolbox in MATLAB 2018a to solve it, and find a set of Pareto solutions of the optimal objective values and the corresponding parameter sets.

References

[1] I. M. Brockman and K. L. J. Prather, "Dynamic metabolic engineering: New strategies for developing responsive cell factories.," *Biotechnology journal*, vol. 10, no. 9, pp. 1360–1369, 2015.

[2] D. Liu, A. A. Mannan, Y. Han, D. A. Oyarzún, and F. Zhang, "Dynamic metabolic control: towards precision engineering of metabolism," *Journal of Industrial Microbiology & Biotechnology*, vol. 45, no. 7, pp. 535–543, 2018.

[3] K. G. Gadkar, F. J. Doyle, J. S. Edwards, and R. Mahadevan, "Estimating optimal profiles of genetic alterations using constraint-based models," *Biotechnology and Bioengineering*, vol. 89, no. 2, pp. 243–251, 2005.

[4] N. Anesiadis, W. R. Cluett, and R. Mahadevan, "Dynamic metabolic engineering for increasing bioprocess productivity," *Metabolic Engineering*, vol. 10, no. 5, pp. 255–266, 2008.

[5] Y. Soma and T. Hanai, "Self-induced metabolic state switching by a tunable cell density sensor for microbial isopropanol production," *Metabolic Engineering*, vol. 30, pp. 7–15, 2015.

[6] A. Gupta, I. M. B. Reizman, C. R. Reisch, and K. L. J. Prather, "Dynamic regulation of metabolic flux in engineered bacteria using a pathway-independent quorum-sensing circuit," *Nature Biotechnology*, vol. 35, no. 3, pp. 273–279, 2017.

[7] S. Klamt, R. Mahadevan, and O. Hädicke, "When Do Two-Stage Processes Outperform One-Stage Processes?," *Biotechnology journal*, vol. 13, no. 2, 2018.

[8] Y. Soma, T. Yamaji, F. Matsuda, and T. Hanai, "Synthetic metabolic bypass for a metabolic toggle switch enhances acetyl-CoA supply for isopropanol production by Escherichia coli," *Journal of Bioscience and Bioengineering*, vol. 123, no. 5, pp. 625–633, 2017.

[9] N. Venayak, K. Raj, R. Jaydeep, and R. Mahadevan, "An Optimized Bistable Metabolic Switch to Decouple Phenotypic States during Anaerobic Fermentation," *ACS Synthetic Biology*, vol. 7, no. 12, pp. 2854–2866, 2018.

[10] P. Dvorak, L. Chrast, P. I. Nikel, R. Fedr, K. Soucek, M. Sedlackova, R. Chaloupkova, V. Lorenzo, Z. Prokop, and J. Damborsky, "Exacerbation of substrate toxicity by IPTG in Escherichia coli BL21(DE3) carrying a synthetic metabolic pathway," *Microbial Cell Factories*, vol. 14, no. 1, pp. 1–15, 2015.

[11] W. Bothfeld, G. Kapov, and K. E. Tyo, "A Glucose-Sensing Toggle Switch for Autonomous, High Productivity Genetic Control," *ACS Synthetic Biology*, vol. 6, no. 7, pp. 1296–1304, 2017.

[12] B. J. Harder, K. Bettenbrock, and S. Klamt, "Temperature-dependent dynamic control of the TCA cycle increases volumetric productivity of itaconic acid production by Escherichia coli," *Biotechnology and Bioengineering*, vol. 115, no. 1, pp. 156–164, 2018.

[13] N. Anesiadis, H. Kobayashi, W. R. Cluett, and R. Mahadevan, "Analysis and design of a genetic circuit for dynamic metabolic engineering," *ACS Synthetic Biology*, vol. 2, no. 8, pp. 442–452, 2013.

[14] T. S. Gardner, C. R. Cantor, and J. J. Collins, "Construction of a genetic toggle switch in Escherichia coli," *Nature*, vol. 403, no. 6767, pp. 339–342, 2000.

[15] D. Angeli, J. E. Ferrell, and E. D. Sontag, "Detection of multistability, bifurcations, and hysteresis in a large class of biological positive-feedback systems.," *Proceedings of the National Academy of Sciences of the United States of America*, vol. 101, pp. 1822–7, mar 2004.

[16] J. E. Ferrell, "Self-perpetuating states in signal transduction: Positive feedback, double-negative feedback and bistability," *Current Opinion in Cell Biology*, vol. 14, no. 2, pp. 140–148, 2002.

[17] C. Hartline, A. Mannan, D. Liu, F. Zhang, and D. Oyarzún, "Metabolite sequestration enables rapid recovery from fatty acid depletion in Escherichia coli," *mBio*, 2020.

[18] A. A. Mannan, D. Liu, F. Zhang, and D. A. Oyarzún, "Fundamental design principles for transcription-factor-based metabolite biosensors," *ACS Synthetic Biology*, vol. 6, no. 10, pp. 1851–1859, 2017.

[19] J. A. J. Arpino, E. J. Hancock, J. Anderson, M. Barahona, G. B. V. Stan, A. Papachristodoulou, and K. Polizzi, "Tuning the dials of synthetic biology," *Microbiology*, vol. 159, pp. 1236–1253, 2013.

[20] Y. Usui, T. Hirasawa, C. Furusawa, T. Shirai, N. Yamamoto, H. Mori, and H. Shimizu, "Investigating the effects of perturbations to pgi and eno gene expression on central carbon metabolism in Escherichia coli using 13 C metabolic flux analysis," *Microbial Cell Factories*, vol. 11, no. 87, pp. 1–5, 2012.

[21] A. von Kamp and S. Klamt, "Growth-coupled overproduction is feasible for almost all metabolites in five major production organisms," *Nature Communications*, vol. 8, no. May, p. 15956, 2017.

[22] A. Gyorgy, J. I. Jiménez, J. Yazbek, H. H. Huang, H. Chung, R. Weiss, and D. Del Vecchio, "Isocost Lines Describe the Cellular Economy of Genetic Circuits," *Biophysical Journal*, vol. 109, no. 3, pp. 639–646, 2015.

[23] Y. Qian, H. H. Huang, J. I. Jiménez, and D. Del Vecchio, "Resource Competition Shapes the Response of Genetic Circuits," *ACS Synthetic Biology*, vol. 6, no. 7, pp. 1263–1272, 2017.

[24] A. Y. Weiße, D. A. Oyarzún, V. Danos, and P. S. Swain, "Mechanistic links between cellular trade-offs, gene expression, and growth," *Proceedings of the National Academy of Sciences*, vol. 112, no. 9, pp. E1038–E1047, 2015.

[25] E. M. Nikolados, A. Y. Weiße, F. Ceroni, and D. A. Oyarzún, "Growth Defects and Loss-of-Function in Synthetic Gene Circuits," *ACS Synthetic Biology*, vol. 8, no. 6, pp. 1231–1240, 2019.

[26] M. Scott, C. W. Gunderson, E. M. Mateescu, Z. Zhang, and T. Hwa, "Interdependence of Cell Growth and Gene Expression : Origins and Consequences," *Science*, vol. 330, no. 6007, pp. 1099–1102, 2010.

[27] A. P. S. Darlington, J. Kim, J. I. Jiménez, and D. G. Bates, "Dynamic allocation of orthogonal ribosomes facilitates uncoupling of co-expressed genes," *Nature Communications*, vol. 9, no. 695, 2018.

[28] H. J. Janßen and A. Steinbüchel, "Fatty acid synthesis in Escherichia coli and its applications towards the production of fatty acid based biofuels.," *Biotechnology for biofuels*, vol. 7, no. 1, p. 7, 2014.

[29] I. M. Keseler, A. Mackie, A. Santos-Zavaleta, R. Billington, C. Bonavides-Martínez, R. Caspi, C. Fulcher, S. Gama-Castro, A. Kothari, M. Krummenacker, M. Latendresse, L. Muñiz-Rascado, Q. Ong, S. Paley, M. Peralta-Gil, P. Subhraveti, D. A. Velázquez-Ramírez, D. Weaver, J. Collado-Vides, I. Paulsen, and P. D. Karp, "The EcoCyc database: Reflecting new knowledge about Escherichia coli K-12," *Nucleic Acids Research*, vol. 45, no. D1, pp. D543–D550, 2017.

[30] S. Marino, I. B. Hogue, C. J. Ray, and D. E. Kirschner, "A methodology for performing global uncertainty and sensitivity analysis in systems biology," *Journal of Theoretical Biology*, vol. 254, no. 1, pp. 178–196, 2008.

Acknowledgements

This work was funded by BBSRC Research Grant BB/M017982/1. We would like to thank Christophe Corre of University of Warwick, UK, and Yoshihiro Toya of Osaka University, Japan, for helpful discussions.

Author contributions

A.A.M. and D.G.B. designed the research, analysed the results and wrote the manuscript. A.A.M. developed the models, performed mathematical analyses and constructed figures.

Competing interest

The authors declare no competing interests.

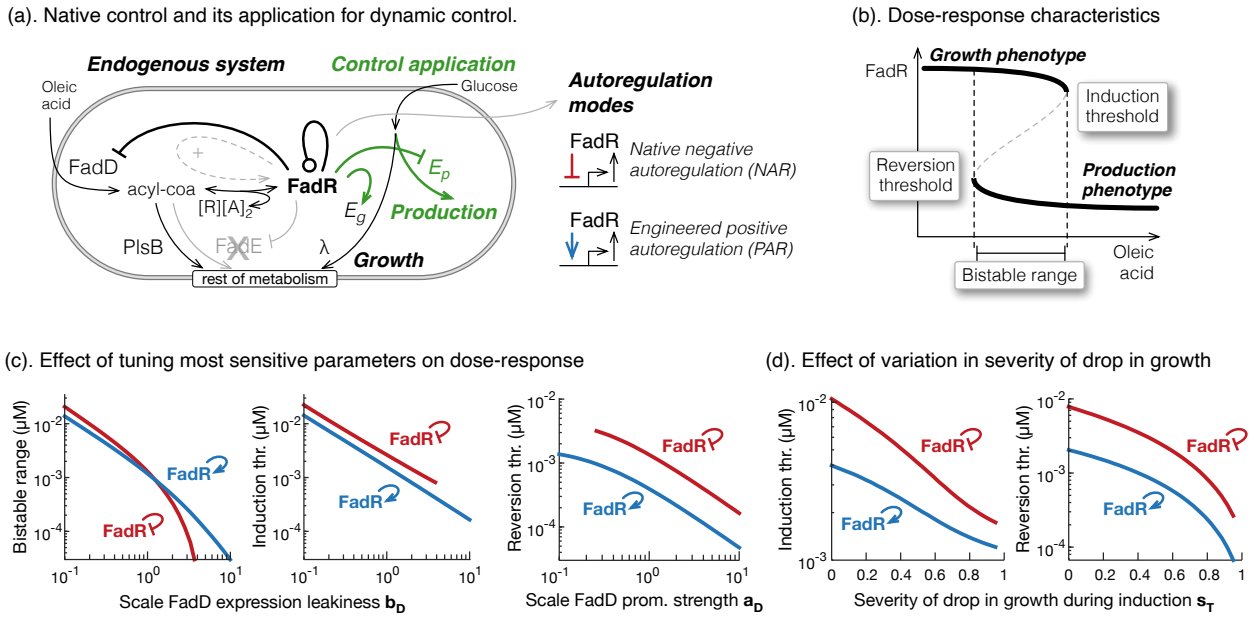

Figure 1: **Design of a robust bistable-switch.** (a). Schematic of the endogenous regulation of fatty acid uptake in *E. coli* DH1Δ*fadE* strain (black text and lines), and how its regulator FadR can be applied to control an oleic acid-induced switch from growth to production (green text and lines). We consider two ways FadR regulates its own expression: the native negative autoregulation (NAR) or engineered positive autoregulation (PAR). (b). Illustration of a dose-response curve and three features we measure to characterise the switch behaviour: induction threshold; reversion threshold and bistable range. (c). Plots of how the bistable range and induction threshold are affected by changes in FadD expression leakiness, and how the reversion threshold is affected by a change in FadD promoter strength, for the native system with NAR (red) and an engineered system with PAR (blue). Parameter were varied from 10%–1000% of their nominal value from Table S2. (d). Plot of how induction and reversion thresholds are affected by changes to the proportional drop in growth rate after induction.

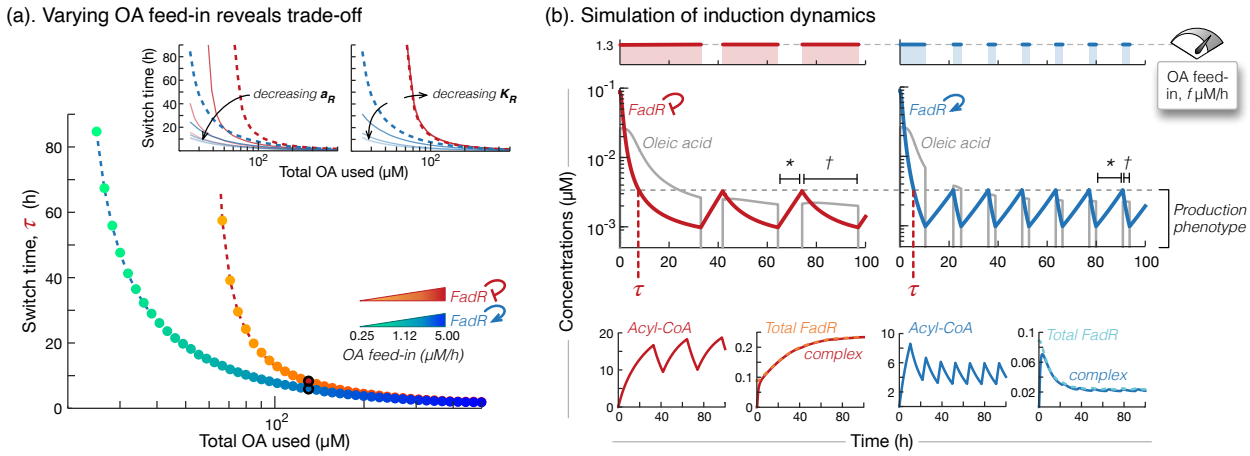

Figure 2: **Tuning inducer feed-in and control circuit to optimise induction process performance.** (a). Plot of the two performance objectives for logarithmic increases in OA feed-in flux from 0.38–5μM/h, of the circuits with NAR (yellow to red dots) and PAR (green to blue dots). Inset plots show how these curves approach a limit when decreasing control circuit FadR promoter strength a_R and affinity to bind its own promoter K_R, from 100% (dashed lines) to 1% (lighter lines) of their nominal values in Table S2. Red curves for system with NAR and blue curves for system with PAR. (b). Simulations of intermittent inductions of OA, at feed-in flux 1.3μM/h (top plots) to retain the production phenotype (middle plots), for the circuits with native NAR (left plots, red curves) and engineered PAR (right plots, blue curves). See Methods for induction program details. We plot availability of OA and dynamic response of FadR (middle plots), and dynamic responses of acyl-CoA, complex, and total FadR (free FadR + complex) (bottom plots). We calculate two induction process performance objectives from these simulations: total OA used (total shaded region in top plots) and switch time (τ in middle plots).

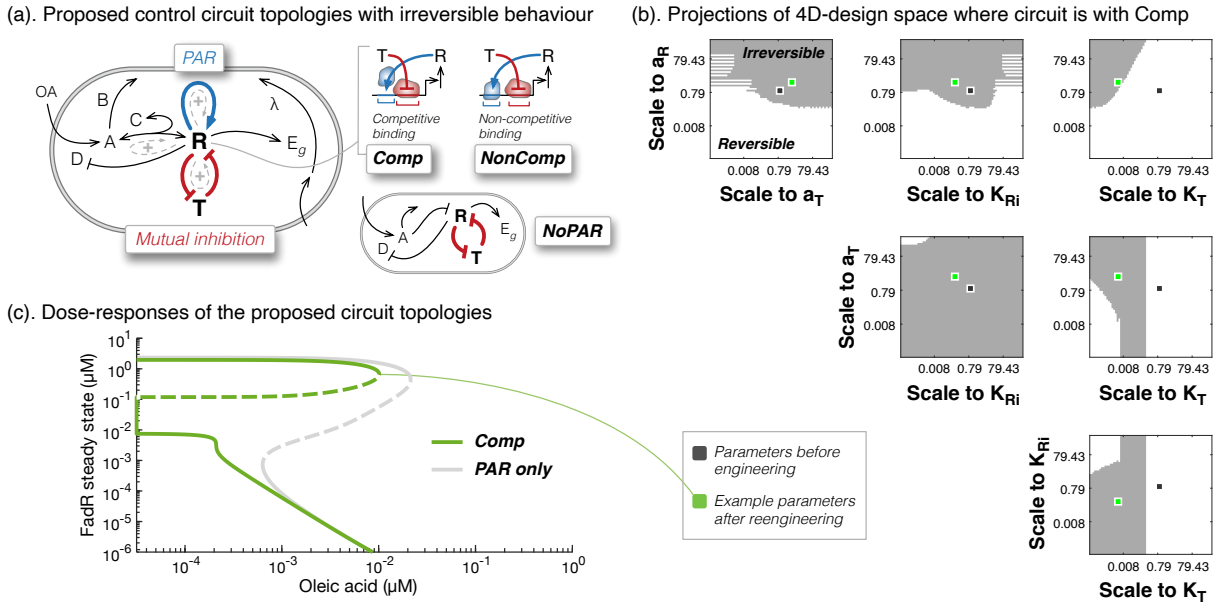

Figure 3: **Augmenting with a positive feedback allows irreversible behaviour.** (a). Schematic of the proposed control circuit with PAR (blue arrow) and an additional positive feedback loop formed from the mutual inhibition between FadR and TetR (red arrows). We consider three possible circuit topologies: where there is no PAR (NoPAR), and where the operator sites of FadR and TetR can be configured so both transcription factors bind competitively (Comp) or non-competitively (NonComp). (b). Plots showing projections of the parameter design space onto every pairwise plane of parameters, for the circuit Comp, the circuit we found has largest design space with irreversible behaviour of the three circuits. We varied parameters a_R, a_T, K_{Ri}, K_T simultaneously between 10^{-3}–10^{3} times their nominal values, and determined irreversible behaviour if we found more than one steady state. The dark spot indicates the nominal parameter set, which did not give an irreversible switch, and the green spot indicates an example parameter regime ($(a_R, a_T, K_{Ri}, K_T) = (0.45,\ 0.26,\ 38.5,\ 22.3)$) that makes switch irreversible (see Table S4 for proposed scaling to parameters). (c) Plot of the dose-response curves showing the irreversible switch behaviour of the Comp circuit, for the example parameter regime (green dot in (b)), and comparison to the circuit with same parameters but with only PAR, as in Fig.1(a).

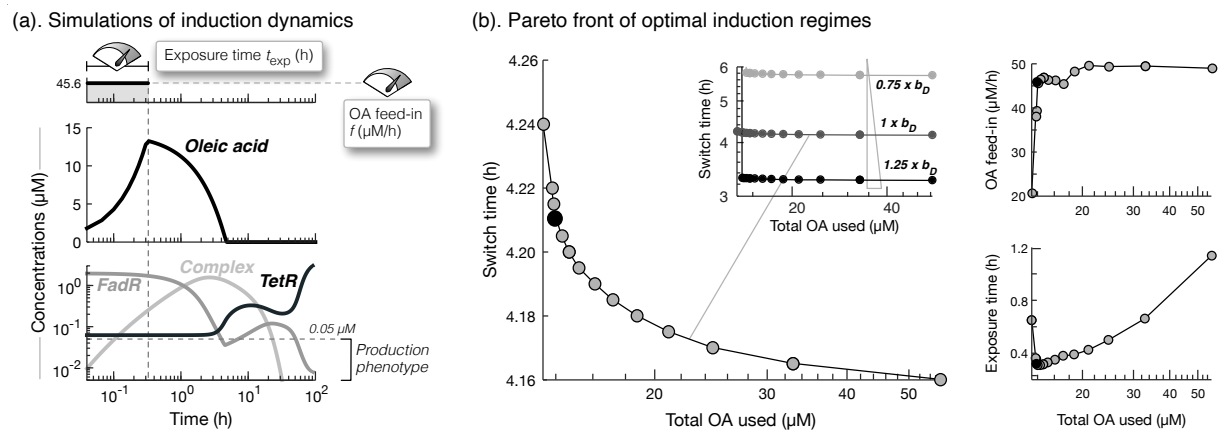

Figure 4: **Tuning induction and irreversible switch to minimise inducer use and switch time.** (a). Simulation of induction with its two tuning dials OA feed-in flux (f) and time length of exposure (t_{exp}) fixed at f=45.6μM/h and t_{exp}=0.31h (top plot). We plot the corresponding dynamic response of oleic acid, free FadR, complex and TetR, over 100 hours of the induction process, also indicating the maximum concentration of FadR of 0.05μM for which we define the cell to be expressing the production phenotype. (b). Plot of the Pareto front of the induction performances achieved (main plot) for optimal feed-in flux and exposure times (right plots), as found from evaluating the multi-objective optimisation problem. The inset plots shows that increasing FadD expression leakiness by as little as 25% b_D can further reduce the switch time with little affect on total OA used.